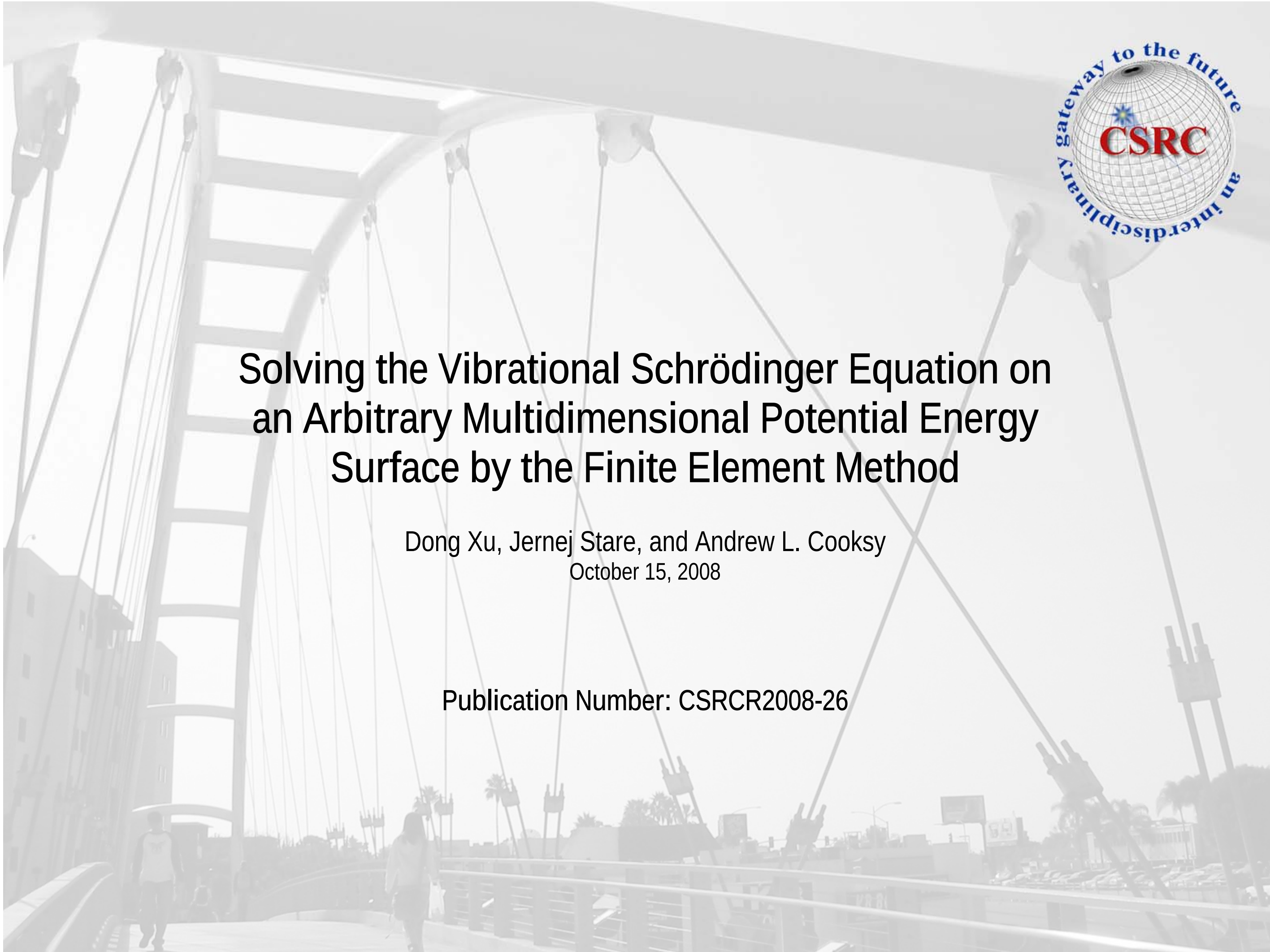

Solving the Vibrational Schrödinger Equation on an Arbitrary Multidimensional Potential Energy Surface by the Finite Element Method

Dong Xu, Jernej Stare, and Andrew L. Cooksy

October 15, 2008

Publication Number: CSRCR2008-26

Computational Science & Engineering Faculty and Students Research Articles

Database Powered by the Computational Science Research Center Computing Group & Visualization Lab

COMPUTATIONAL SCIENCE & ENGINEERING

SAN DIEGO STATE UNIVERSITY

Computational Science Research Center
College of Sciences
5500 Campanile Drive
San Diego, CA 92182-1245
(619) 594-3430

Solving the Vibrational Schrödinger Equation on an Arbitrary Multidimensional Potential Energy Surface by the Finite Element Method

Dong Xu

National Biomedical Computation Resource,

University of California, San Diego,

La Jolla, California 92093-0505, USA

Jernej Stare

National Institute of Chemistry, Hajdrihova 19, 1000 Ljubljana, Slovenia

Andrew L. Cooksy*

San Diego State University, San Diego, California 92182-1245 USA and

Centro de Graduados e Investigación del Instituto Tecnológico de Tijuana,

Apdo Postal 1166, Tijuana, B.C., México

(Dated: October 9, 2008)

Abstract

A computational protocol has been developed to solve the bounded vibrational Schrödinger equation for up to three coupled coordinates on any given effective potential energy surface (PES). The dynamic Wilson G-matrix is evaluated from the discrete PES calculations, allowing the PES to be parametrized in terms of any complete, minimal set of coordinates, whether orthogonal or non-orthogonal. The partial differential equation is solved using the finite element method (FEM), to take advantage of its localized basis set structure and intrinsic scalability to multiple dimensions. A mixed programming paradigm takes advantage of existing libraries for constructing the FEM basis and carrying out the linear algebra. Results are presented from a series of calculations confirming the flexibility, accuracy, and efficiency of the protocol, including tests on FHF^{-}, picolinic acid N-oxide, *trans*-stilbene, a generalized proton transfer system, and selected model systems.

I. INTRODUCTION

The dynamics of any chemical change in a molecular system corresponds to motion along an effective potential energy surface (PES), parametrized by some choice of vibrational coordinates. In relatively rigid molecules at low vibrational excitation, motion along these coordinates is often accurately modeled by a collection of decoupled simple harmonic oscillators. However, this approximation fails to describe many problems of interest, including hindered internal rotations, bends and stretches of hydrogen-bonded atoms, and van der Waals vibrations. Of relevance to our research are the family of free radicals involving coupling between the unpaired electron(s) and a conjugated π-system, particularly in unsaturated carbon-chain or monocyclic hydrocarbon intermediates. In these cases, the structure of the radical intermediate may differ substantially from that of the parent compound, and the redistribution of electron spin along the conjugated π-system may lead to shifts from the anticipated location of the principal reactive site.[1–5] The PES for motion along this coordinate of spin "relocalization" may feature extensive flat regions, multiple minima, and strongly coupled vibrational modes. Relevant surfaces may be parametrized in terms of bond lengths, bond angles, dihedral angles, or any linear combination thereof.

Our goal has been to solve the vibrational Schrödinger equation (VSE) for a polyatomic molecule, starting from an arbitrary PES of up to three dimensions, without requiring the selection of specific coordinates or basis functions. The wavefunctions and energies obtained from these calculations may then be used to predict vibrational spectra involving strongly coupled and anharmonic modes. Although many pathological vibrational problems of three or more dimensions have been tackled over the last twenty years, the approaches tend to tailor the Hamiltonian, the coordinate system, and/or the basis set to the particular problem. This paper presents a general procedure for solving the bounded VSE on an arbitrary PES, based on the finite element method (FEM), and demonstrates its straightforward application to a diverse range of problems in vibrational analysis.

Of many candidate algorithms for solving the Schrödinger equation in several dimensions, FEM benefits by virtue of its local approximation properties. As in most numerical methods, FEM discretizes continuous functions, often onto a regularly spaced grid. A common obstacle to solving the VSE in several dimensions is the reconstruction of highly peaked wave functions, because a uniformly fine multidimensional grid is computationally expensive.

FEM addresses this challenge by discretizing the spatial wave function into polyhedra, with linear combinations of local polynomial functions defined on these polyhedra, and adapting the multidimensional mesh to the solution. The approximation can be improved if necessary through a manual refinement of the mesh, while an estimator for the local approximation errors selects the relevant elements to be refined. The combination of an efficient FEM and an adaptive mesh generation scheme results in a general method to predict vibrational dynamics on an arbitrary, multidimensional PES.

Its adaptability to complex problems and unusual geometries has made FEM popular for problems in classical dynamics, and it has seen many recent applications to quantum electronic structure calculations, particularly of quantum dots.[6–8] Its application to vibrational quantum mechanics has been sporadic, although its success in solving the 2D methyl bending vibrational states of toluene dates from 1978.[9] Only some 20 papers have pursued this application since then, and to our knowledge the only use of FEM in vibrational quantum mechanics in the last five years is in a 3D solution to the vibrational dynamics of the O_2-H_2O van der Waals complex.[10,11]

We have combined existing, open-source math libraries with programs and scripts to arrive at a single package – incorporating various programs, libraries, and scripts – for solving the general VSE in up to three dimensions. This report presents the design details and benchmark results of this methodology for the solution of the VSE on several surfaces of two and three dimensions.

II. METHODS

The method is intended for application to a highly coupled and anharmonic subset of a molecule's vibrational degrees of freedom, which are then sufficiently decoupled from any other vibrational modes. The relaxed, pointwise PES is typically based on a scan of partial geometry optimizations, using a large series of electronic structure calculations holding the vibrational coordinates of interest fixed at specific values. However, there is no requirement that the PES be strictly *ab initio*, nor even based on explicit calculations at each point. Empirical, analytical expressions for couplings can greatly reduce the computational investment in developing PES's of high dimensionality, and more advanced approaches include the use of local coupled cluster methods.[12]

Given such a surface of M dimensions, our general approach to solve the multidimensional VSE proceeds as follows: (a) Calculate each element of the $M \times M$ Wilson G-matrix at each point on the PES; (b) Fit M-dimensional analytical surfaces (of arbitrary complexity) to the geometry-dependent values for the potential energy and for each G-matrix element; (c) Derive the corresponding kinetic energy operator $\hat{T}$ in terms of the analytical form of the Wilson G-matrix; (d) Construct a fine-grain Hamiltonian matrix using basis sets and boundary conditions established by FEM and solve for the desired eigenvalues and eigenvectors. These steps are detailed below.

In order to take advantage of existing libraries, a mixed programming paradigm is chosen. Scripts were written in Python to glue existing components developed in different high-performance programming languages such as C++ and Fortran, and to handle labor intensive tasks such as manipulation and management of the molecular structure and energy data files.

A. Determination of the Wilson G-matrix

Each point on the PES is associated with a specific distribution of all the nuclei. To restrict ourselves to a purely vibrational problem, we enforce the Eckart conditions[13] at each of these points:

$$\sum_{i=1}^{N} m_i \, (\vec{d}_i \cdot \vec{r}_i^{\,0}) = 0 \tag{1}$$

$$\sum_{i=1}^{N} m_i \, (\vec{d}_i \times \vec{r}_i^{\,0}) = 0, \tag{2}$$

where $\vec{r}_i^{\,0}$ denotes the position vector of the ith atom in the reference geometry (with origin at the molecular center of mass) and $\vec{d}_i$ is its displacement vector relative to the reference geometry, and N is the total number of nuclei.

The vibrational Hamiltonian may be written in general form

$$\hat{H}^{\mathrm{vib}} = \hat{T}^{\mathrm{vib}}(\vec{R}) + E^{\mathrm{eff}}(\vec{R}), \tag{3}$$

or in terms of Cartesian coordinates of the atoms,

$$\hat{H}^{\mathrm{vib}} = -\frac{\hbar^2}{2} \sum_{i=1}^{3N} \frac{1}{m_i} \frac{\partial^2}{\partial x_i^2} + V, \tag{4}$$

where m_i is the mass of the nucleus associated with the ith Cartesian coordinate x_i, and where V is the potential energy.

The kinetic energy operator in generalized local coordinates is more complex than in Cartesian or normal mode coordinates,[14–16] containing mixed derivative terms as well as the G matrix of Wilson *et al.*[14,15] The G matrix is symmetric, with matrix elements G^{rs} corresponding roughly to reciprocal reduced masses:

$$G^{rs} = \sum_{i=1}^{3N} \frac{1}{m_i} \frac{\partial q_r}{\partial x_i} \frac{\partial q_s}{\partial x_i}. \tag{5}$$

Alexandrov *et al.*[17] introduced an approach to solving the G matrix by first calculating the elements of the inverse G matrix, having elements G_{rs}, where

$$G_{rs} = \sum_{i=1}^{3N} m_i \frac{\partial x_i}{\partial q_r} \frac{\partial x_i}{\partial q_s}. \tag{6}$$

This approach retains the couplings between all possible pairs of internal and Cartesian coordinates (q_r and x_i), which may otherwise be obscured by imposition of the Eckart conditions during direct evaluation of Eq. 5.[18]

For each value of q_s, each of the atomic Cartesian coordinates x_i is a 1D spline interpolated along q_r, and the derivatives are evaluated at each of the q_r values. The same procedure is repeated with changed roles between q_r and q_s in order to obtain $\partial x_i/\partial q_s$. The G_{rs} matrix elements are calculated by Stare's GMAT program,[19,20] using Eq. 6 for *each* optimized structure on the PES, and the G^{rs} elements are obtained by inverting the matrix of G_{rs}.

B. Fitting surfaces to pointwise V and G-matrix values

The Hamiltonian matrix involves derivatives of the potential energies and of the G-matrix elements. For the present work, those were obtained from analytical surfaces written as functions of the vibrational coordinates of interest. Therefore, the pointwise potential energies and G-matrix elements obtained from electronic structure calculations are fitted into a multi-dimensional analytic function using non-linear least squares regression algorithms such as the Gauss-Newton[21] or Levenberg-Marquardt methods.[22,23]

In general, a set of pre-defined non-linear equations may be fit to the pointwise PES, and ranked by a quality index such as the R^2 value. The TableCurve 3D package[24] provides this capability for surfaces of two dimensions. For higher dimensionality, NLREG (Non-Linear Regression Analysis) offers a scripting environment capable of handling as many as 2000 independent variables, 2000 parameters, and arbitrary dimensionality.[25] However, determination of an adequate functional form is likely to require substantial effort. In this work, the model potentials already have an analytical form. Pointwise 2D PES's were fitted using TableCurve 3D, and 3D surfaces using a series of 2D surface fits and a spline interpolation of the resulting fitting parameters.

C. Formulation of $\hat{T}$ in internal coordinates

To rewrite Eq. 4 for a set of generalized coordinates $\{q\}$, Podolsky[16] and others[26,27] showed that the kinetic energy operator may take the form

$$\hat{T}_q = -\frac{\hbar^2}{2}\sum_{r=1}^{M}\sum_{s=1}^{M}\left\{j^{-1/2}\frac{\partial}{\partial q_r}\left[j\cdot G^{rs}\frac{\partial}{\partial q_s}\left(j^{-1/2}\right)\right]\right\}, \tag{7}$$

where M is the number of coordinates taken into account and where j is the determinant of the Jacobian transformation matrix between $\{x\}$ and $\{q\}$:

$$j = \det|J_{ij}|, \quad J_{ij} = \partial x_i/\partial q_j. \tag{8}$$

Unlike its Cartesian analog, the kinetic energy operator in Eq. 7 includes mixed second derivatives: the kinetic coupling terms. Moreover, all of the terms j, $j^{-1/2}$, and G^{rs} are, in general, functions of the coordinates in the set $\{q\}$; thus, they should be included in the differentiation.

By expanding Eq. 7, the kinetic operator can also be written as

$$\begin{aligned}\hat{T}_q &= -\frac{\hbar^2}{2}\sum_{r=1}^{M}\sum_{s=1}^{M}\left\{\frac{\partial}{\partial q_r}\left[G^{rs}\frac{\partial}{\partial q_s}\right]-\left[G^{rs}\frac{\partial}{\partial q_r}\frac{\partial}{\partial q_s}\right]\right\}\\ &= -\frac{\hbar^2}{2}\sum_{r=1}^{M}\sum_{s=1}^{M}\left\{\frac{\partial}{\partial q_r}\left[G^{rs}\frac{\partial}{\partial q_s}\right]\right\}+V'(q),\end{aligned} \tag{9}$$

where $V'(q)$ is the extrapotential[28] or pseudopotential[29–31] term which has been shown to be negligible[32] because the coordinate dependence of the Jacobian determinant, j, is much smaller than the dependence of a particular individual component G^{rs}.[29] Equation 9 then takes on the simplified form

$$\hat{T}_q \approx -\frac{\hbar^2}{2}\sum_{r=1}^{M}\sum_{s=1}^{M}\left[G^{rs}\frac{\partial^2}{\partial q_r\partial q_s}+\frac{\partial G^{rs}}{\partial q_r}\frac{\partial}{q_s}\right]. \tag{10}$$

A further approximation could be to assume that the elements of the Wilson G-matrix are constant:

$$\hat{T}_q \approx -\frac{\hbar^2}{2}\sum_{r=1}^{M}\sum_{s=1}^{M}\left[G^{rs}\frac{\partial^2}{\partial q_r \partial q_s}\right]. \tag{11}$$

Alternatively, we could retain the coordinate dependence of the Wilson G-matrix elements, but neglect the kinetic coupling terms. Hence, by omitting the mixed second derivatives from Eq. 7, we obtain

$$\hat{T}_q \approx -\frac{\hbar^2}{2}\sum_{r=1}^{M}\sum_{s=1}^{M}\frac{\partial}{\partial q_r}\left[G^{rs}\frac{\partial}{\partial q_r}\right]. \tag{12}$$

Finally, we may combine both the *constant-G* and the *no kinetic coupling* approximations, yielding an expression similar in form to the Cartesian form of the Hamiltonian (Eq. 4):

$$\hat{T}_q \approx -\frac{\hbar^2}{2}\sum_{r=1}^{M}\sum_{s=1}^{M}\left[G^{rs}\frac{\partial^2}{\partial q_r^2}\right]. \tag{13}$$

Among the possible levels of simplification of the original Podolsky expression for the kinetic energy operator (Eq. 7), the one yielding Eq. 10 is reasonable and generally acceptable. This is, however, not always true for the *constant-G* and the *no kinetic coupling* approximations (Eqs. 11–13). This work uses the kinetic energy operator given in Eq. 10, unless stated otherwise, allowing any minimal and complete coordinate set $\{q\}$ to be used.

Furthermore, the treatments represented by Eqs. 10–13 may readily be generalized to encompass the exact forms in Eqs. 7 and 9, in case the approximate forms give rise to significant errors. Lauvergnat and Nauts[33,34] have developed a numerical scheme to compute the exact kinetic energy operator in curvilinear coordinates, which may be employed in conjunction with the FEM scheme to give solutions to any given precision.

D. Solution using FEM

A grid-based method was adopted in this work so as to avoid presuming any particular functional form for the wavefunctions, such as a linear combination of harmonic oscillator eigenfunctions. Even within grid-based methods, there remain several choices for solving the vibrational Schrödinger equation. Limitations on the plane-wave modeling of electronic wavefunctions inspired the development of various real-space approaches, including finite difference methods (FDM) and FEM,[35–37] which produce sparse, structured Hamiltonian matrices, require no Fourier transforms, and allow some degree of variable resolution in real space. However, to achieve these advantages, FDM relinquishes the use of a basis set and works instead by discretizing individual terms of the equation of interest on a real-space grid. As a result, quantities of interest are defined only at discrete points in space, limiting the accuracy of integrations and complicating the handling of electron potentials. As a further consequence, the FDM is not variational; the error can be of either sign and convergence is often from lower energy.

Finite element methods achieve the significant advantages of FDM without conceding the use of a basis. Like the plane wave method, FEM is a variational expansion method, but the basis functions are strictly local, piecewise polynomials. Because the basis is composed of polynomials, it is completely general and the convergence of the method can be controlled systematically by increasing the number (h) and/or polynomial order (p) of the basis functions (*hp* refinement). Because the basis functions are strictly local in real space, FEM achieves the advantages of FDM approaches: (*i*) The method produces sparse, structured matrices, which in turn enable the effective use of iterative solution methods; (*ii*) The method requires no Fourier transforms, as all calculations are performed in real space; (*iii*) The method allows for variable resolution in real space more so than FDM approaches by increasing the number or polynomial order of the basis functions where needed. The FEM thus combines the significant advantages of both real-space-grid and basis-oriented approaches.

The application of discrete variable representation (DVR) methods to problems of high dimensionality has been limited to some extent by difficulties in constructing effective multidimesional basis sets within the narrow DVR constraints.[38,39] A direct comparison between the FEM and a modified DVR approach to predicting the rotational energy levels of H_2O and H_3O^+ found the two methods to be comparable.[40] Schneider and Collins have devised a finite element DVR method (FEDVR) that combines the advantages of two discretization methods: the intrinsic accuracy of DVR using a well-chosen basis set, and the highly sparse matrices and adaptive grid capabilities of FEM.[41] The goal of the present work is a more general approach, at the cost of some computational efficiency.

The major disadvantages of FEM are overcome by ongoing improvements in software and hardware. First, the matrices produced by FEM tend to be less sparse, and often less simply structured, than those produced by FDM, and these matrices must be stored, leading to increased memory and I/O requirements. However, the storage requirement for eigenvectors scales quadratically with system size, while the storage requirement for the FEM matrices scales only linearly. Thus, the significance of this disadvantage decreases with increasing system size. As a second drawback, FEM produces generalized eigenvalue problems rather than the standard problems produced by many FDM approaches. Finally, FEM can be more difficult to implement than either FDM or plane wave approaches. However, the hardware-related demands such as memory size, matrix storage space, and cpu time for less sparse matrices may be distributed by parallel processing, for which FEM is ideally constructed. The second and third challenges above are addressed by using user-friendly finite element libraries such as LibMesh[42] in combination with an efficient iterative eigenvalue solver based on the Davidson or Lanczos algorithms.

General 2D and 3D mesh-based electronic structure representations using finite element methods as approximate numerical schemes for partial differential operators have become widely used in only the last ten years, and have proven to be efficient and accurate tools in many electronic structure calculations.[18]). No substantial adjustment of codes or scripts is required to change the dimensionality of the problem in FEM, allowing a wide range of systems to be studied with the same software.

1. *Formulation of the Schrödinger Equation*

For a generalized time-independent Schrödinger equation, we wish to solve

$$-\nabla^2 u + Vu - \epsilon u = 0, \tag{14}$$

where V is the arbitrary potential energy surface and ϵ is the vibrational energy eigenvalue. In order to use FEM, we require an equivalent weak or variational formulation of Eq. 14. Taking the inner product of the differential equation with an arbitrary test function ν yields an equivalent integral equation. We assume that all functions involved are sufficiently regular to keep the integrals well defined, as will be the case in our applications:

$$\int_\Omega \nu \left[-\nabla^2 u + Vu - \epsilon u\right] d\Omega = 0, \tag{15}$$

where we denote the domain by Ω. Strang and Fix provide details regarding the relevant function spaces.[43] To reduce the order of the highest derivative and create a boundary term, we then integrate the ∇^2 term by parts:

$$\int_\Omega \nabla\nu \cdot \nabla u \, d\Omega - \int_\Gamma \nu \nabla u \cdot \hat{n} \, d\Gamma + \int_\Omega \nu \left[(V - \epsilon)u\right] \, d\Omega. \tag{16}$$

The boundary surface is denoted by Γ and $\hat{n}$ is the outward unit normal vector.

For a quantum state bounded in all dimensions, the wavefunction u converges to zero at the boundary of the domain, and therefore satisfies the homogeneous Dirichlet boundary condition,

$$u = 0 \text{ on } \partial\Omega = \Gamma. \tag{17}$$

As a result, the surface integral in Eq. 16 vanishes. The differential formulation Eq. 14 is then equivalent to the following weak formulation: find the scalars ϵ and functions u such that

$$\int_\Omega \nabla\nu \cdot \nabla u \, d\Omega + \int_\Omega \nu V u \, d\Omega = \epsilon \int_\Omega \nu u \, d\Omega. \tag{18}$$

The original problem Eq. 14 is thus reformulated in such a way that the highest derivative which occurs is of order 1, and the homogeneous boundary condition is naturally imposed, having been built into the equation itself. The problem is now in a form which is suitable for approximate solutions by FEM. Because all integrands of such functions (and their linear combinations) will have at most finite discontinuities at interelement boundaries, the integrals are straightforward to evaluate as sums of integrals over individual elements.

The kinetic energy operator in Eq. 10 is derived for the vibrational Hamiltonian represented by a set of active internal coordinates. Thus the full VSE can be written as

$$\left\{ -\frac{1}{2} \sum_{r=1}^{M} \sum_{s=1}^{M} \left[G^{rs} \frac{\partial^2}{\partial q_r \partial q_s} + \frac{\partial G^{rs}}{\partial q_r} \frac{\partial}{\partial q_s} \right] + V(Q) \right\} \psi = \epsilon \psi. \tag{19}$$

The difference between Eq. 19 and the general time-independent formula in Eq. 18 is the kinetic energy operator, which contains second-order mixed derivative terms and G-matrix elements instead of a Laplacian. Since the G-matrix elements G^{rs} are coordinate-dependent, non-linear analytic functions, their derivatives with respect to the individual coordinates are readily incorporated into the Hamiltonian.

Applying similar procedures described above, we obtain the weak formulation for Eq. 19:

$$\int_\Omega \sum_{r=1}^{M} \sum_{s=1}^{M} \left[G^{rs} \frac{\partial u}{\partial q_r} \frac{\partial \nu}{\partial q_s} + \nu \frac{\partial G^{rs}}{\partial q_r} \frac{\partial u}{\partial q_s} \right] \, d\Omega + \int_\Omega \nu V u \, d\Omega = \epsilon \int_\Omega \nu \, u \, d\Omega. \tag{20}$$

To find an approximate solution, we apply Galerkin's approach[44,45]:

$$u = \sum_j c_j \phi_j \text{ and } \nu = \sum_i b_i \phi_i, \tag{21}$$

where $\{\phi_k\}_{k=1}^n$ is a real FEM basis satisfying the essential boundary condition, and where $\{c_j\}$ and $\{b_i\}$ are the expansion coefficients. Then Eq. 18 becomes

$$\sum_i b_i \sum_j c_j \int_\Omega \left[\nabla\phi_i \cdot \nabla\phi_j + V\phi_i\phi_j\right] d\Omega = \sum_i b_i \epsilon \sum_j c_j \int_\Omega \phi_i\phi_j \, d\Omega \quad \forall\{b_i\}, \tag{22}$$

or, identifying matrix elements,

$$\sum_i b_i \sum_j c_j A_{ij} = \sum_i b_i \epsilon \sum_j c_j M_{ij} \quad \forall\{b_i\}, \tag{23}$$

which implies

$$\sum_j c_j A_{ij} = \epsilon \sum_j c_j M_{ij} \quad i = 1 \ldots n, \tag{24}$$

due to the arbitrariness of $\{b_i\}$. We have arrived at a generalized eigenproblem determining the approximate eigenvalues ϵ and eigenfunctions $u = \sum c_j \phi_j$ of the weak formulation, and thus of the original problem:

$$\boldsymbol{A}\boldsymbol{c} = \epsilon \boldsymbol{M}\boldsymbol{c}, \tag{25}$$

where

$$A_{ij} = \int_\Omega \left[\nabla\phi_i \cdot \nabla\phi_j + V\phi_i\phi_j\right] d\Omega$$

and

$$M_{ij} = \int_\Omega \phi_i\phi_j \, d\Omega.$$

$\boldsymbol{A}$ is the global stiffness matrix and $\boldsymbol{M}$ is the global mass matrix. As in the plane wave method, given the expansion of the potential, the above matrix elements can be evaluated exactly due to the polynomial nature of the basis. As in the FDM, the above matrices are sparse, symmetric, and structured due to the strict locality of the basis.

To put this in terms of the G-matrix elements, Eq. 20 becomes

$$\begin{aligned}\sum_i b_i \sum_j c_j \int_\Omega \sum_{r=1}^{M}\sum_{s=1}^{M} \Bigg[G^{rs} \frac{\partial\phi_i}{\partial q_r}\frac{\partial\phi_j}{\partial q_s} \\ + \phi_i \frac{\partial G^{rs}}{\partial q_r}\frac{\partial\phi_j}{\partial q_s}\Bigg] d\Omega + \int_\Omega V\phi_i\phi_j \, d\Omega = \sum_i b_i \sum_j c_j \epsilon \int_\Omega \phi_i\phi_j \, d\Omega.\end{aligned} \tag{26}$$

which is equivalent to the generalized eigenproblem, Eq. 25, where now

$$A_{ij} = \int_{\Omega} \left\{ \sum_{r=1}^{M} \sum_{s=1}^{M} \left[G^{rs} \frac{\partial \phi_i}{\partial q_r} \frac{\partial \phi_j}{\partial q_s} + \phi_i \frac{\partial G^{rs}}{\partial q_r} \frac{\partial \phi_j}{\partial q_s} \right] + V \phi_i \phi_j \right\} d\Omega. \tag{27}$$

The sparse and symmetric properties of the global matrices are preserved as a result of the symmetric G-matrix and the symmetric formulation of the kinetic energy terms.

The vibrational eigenvalues and eigenfunctions are obtained by solving the generalized eigenvalue problem in Eq. 20, and the resulting eigenvectors, ψ_ϵ, are normalized according to

$$\int_{\Omega} |\psi_\epsilon|^2 \, d\Omega = 1. \tag{28}$$

2. The Finite-Element Basis

Finite-element bases are well-chosen sets of strictly local, piecewise polynomials, and have an extensive literature.[43,46–48] The above transformations are affine and invertible, permitting the construction of efficient meshes that concentrate relatively small elements (and thus basis functions) where needed. Global basis functions $\{\phi_i\}$ of the method are generated by piecing together local basis functions at interelement boundaries, according to a scheme which is recorded in a connectivity table, using the correspondence between nodes in the local and global bases. Efficient assembly of the finite element matrices relies on the local-to-global translation provided by the connectivity table.

It is not difficult in 1D to define local bases that match in value at interelement boundaries, but this is less straightforward in higher dimensions, where continuity across interelement curves or surfaces must be achieved. This has led to a wide variety of choices and a corresponding literature.[48] Nevertheless, because the basis functions are strictly local, the matrices are sparse and the method is reliably scalable. Furthermore, the basis functions within each element are low-order polynomials, and hence computationally efficient. Although higher-order polynomials are possible for finite element bases in multiple dimensions, it becomes increasingly difficult to match both values and derivatives across entire curves or surfaces, constraining the available meshes. In higher dimensions, however, there arises a significant additional choice of shapes. The most common 2D element shapes are triangles and quadrilaterals. In 3D, tetrahedra, hexahedra, and prisms are among the most common. And with multiple shapes available, individual domains are often partitioned into multiple different shapes, for example, both triangles and quadrilaterals. In the context of molecular vibration calculations, however, the domain is simple, rectangular cells, and our first choice has been the hexahedral elements.

3. *Solution to the Generalized Eigenvalue Problem*

Numerous algorithms for solving the generalized matrix eigenvalue problem in Eq. 20 are available. When the global matrices are not too large, the eigenvalues and eigenvectors can be determined easily by performing Givens and Householder transformations.[49] However, these transformations have the disadvantage of producing extra non-zero matrix elements, and worse, the cost of the calculation scales as N^3 where N is the size of the matrix. The performance of the direct method thus becomes debilitating when treating a large system in three dimensions. Our choice of algorithm, due to the large and sparse nature of the global matrices, favors iterative methods that preserve the structure of the matrices and access them only via matrix-vector multiplications. Since most of the time we are only interested in a portion of the eigenvalue spectrum, subspace methods are ideal for this task. These are iterative methods that build a search subspace from which the eigenvector approximations are selected. In the symmetric case, this is usually done using a Rayleigh-Ritz step. In each iteration the search subspace is expanded by one or more new search directions. Restarted subspace methods limit the dimension of the search subspace by periodically discarding some search direction. In the present work, we relied primarily on an eigensolver based on a variant of the Jacobi-Davidson (JD) algorithm,[50] which is optimized for the generalized symmetric eigenvalue problem on single-processor workstations. We also tested the Implicitly Restarted Lanczos algorithm (IRL), implemented in the ARPACK and Parallel ARPACK (PARPACK) packages,[51] which is constructed for execution in a distributed computing environment.

Details of our implementation of the LibMesh library are given in Appendix A, and relevant aspects of the JDSYM eigensolver are described briefly in Appendix B. The calculations were carried out primarily using 2 GHz Opteron/Linux processors with up to 3 GB RAM. Three-dimensional calculations demanded at least 2 GB of RAM, and up to 2 hours of cpu time for the eigensolution step, using the grid dimensions given in the following section.

III. RESULTS AND DISCUSSION

This package has been tested on numerous one-dimensional problems, including comparison to results from our previous study of the tolane internal rotation using the Numerov method.[52] Greater interest is attached to the more demanding multidimensional problems, however, and only those are described below.

a. Harmonic Oscillators. We first tested the method on 2D and 3D harmonic oscillators, with energy functions

$$V = \sum_{i=1}^{M} k_i x_i^2 \qquad E = \sum_{i=1}^{M} \sqrt{k_i} \left(v_i + \frac{1}{2} \right), \tag{29}$$

with M the number of dimensions. These potentials were chosen for their simplicity, relevance to typical molecular systems, and in the isotropic case (all k_i equal) to verify the method's ability to correctly identify and distinguish degenerate states.

For comparison to previous work, our protocol was also tested on the 3D anisotropic harmonic potential where $k_x = 1, k_y = 1.44, k_z = 1.69$. Our results are shown in Table I along with previous results calculated by FDM[53] and FEM[54] methods. The element volumes are specified by the shape type and number of nodes; for example, HEX27 is a hexahedral basis function with 27 nodes. The impact of polynomial order and type on the convergence is evident when comparing our results with the results calculated by Ackermann *et al.* The energy calculated using linear shape functions is worse than any results calculated at higher polynomial order. The better results they obtain with the quadratic shape function level may be attributed to their adaptive mesh refinement (AMR), which allows calculation of a specific eigenvalue to high precision. In the context of molecular vibrations, however, we often need to calculate tens or hundreds of eigenvalues at one time. Global (but manual) *hp* refinement provided with the present software, in conjunction with a diverse selection of element types, provides an additional flexibility that partly compensates for the lack of AMR. We find also that, using cubic shape functions, the Hermite polynomial produces more accurate results than the Lagrange polynomial, which demonstrates the advantage of using shape functions with C^1 continuity over C^0. Although Ackermann *et al.* also achieved highly accurate results using quintic ($p = 5$) Lagrange polynomials, these shape functions become computationally quite expensive when $p \geq 4$; thus they are rarely used in practical applications. We note that the present package calculates eigenvalue 202 with good

TABLE I: Selected Eigenvalues of the 3D Anisotropic Harmonic Oscillator ($k_x = 1, k_y = 1.44, k_z = 1.69$).

n	$(v_x v_y v_z)$	exact	FEM HEX27[a]	FEM HEX8[b]	FEM/AMR[c]	FDM[d]
1	(0 0 0)	1.75	1.7501603438	1.7500020614	1.75112123	1.7452
2	(1 0 0)	2.75	2.7503539601	2.7500047973	1.75000532	2.7399
3	(0 1 0)	2.95	2.9504927697	2.9500074904	1.75000045	2.9381
4	(0 0 1)	3.05	3.0505816415	3.0500093822		3.0372
5	(2 0 0)	3.75	3.7509261465	3.7500150688		
6	(1 1 0)	3.95	3.9506863860	3.9500102262		3.9327
7	(1 0 1)	4.05	4.0507752578	4.0500121179		4.0314
8	(0 2 0)	4.15	4.1514722542	4.1500276821		
9	(0 1 1)	4.25	4.2509140674	4.2500148108		4.2284
10	(0 0 2)	4.35	4.3518211405	4.3500364903		
...						
202	(4 4 4)	15.75		15.75051443		

[a]This work, quadratic Lagrange polynomials on $30 \times 30 \times 30$ HEX27 elements.
[b]This work, cubic Hermite polynomials on $30 \times 30 \times 30$ HEX8
[c]Adaptive FEM by Ackermann *et al.*,[54] the three ground state energies are calculated with linear, quadratic and cubic Lagrange polynomials on TET10 elements respectively.
[d]Alvarez-Collado and Buenker.[53]

precision, to show that this approach is suitable for application to highly excited vibrational eigenstates.

b. 2D Coupled Anharmonic Sextic Oscillator. As an initial test on a coupled system, the potential for two coupled anharmonic sextic oscillators was used:

$$V(x, y) = V_6(x) + V_6(y) + xy, \qquad V_6(q) \equiv \frac{q^2}{2} + 2q^4 + \frac{q^6}{2}. \tag{30}$$

We calculated the lowest 13 eigenstates and eigenvalues using cubic Hermite polynomials on a 200×200 QUAD8 grid in $[-4, 4] \times [-4, 4]$. Braun *et al.*[55] have also used this system to test their efficient Chebyshev-Lanczos method. The results for the eigenvalues are shown in Table II. The low-lying binding energies are in good agreement with the results of Kaluza[56] and Braun *et al.*,[55] both obtained using the Lanczos method.

TABLE II: Lowest 13 Eigenvalues of the 2D Coupled Sextic Anharmonic Oscillators

i	analytical Lanczos[c]	Chebyshev/ Lanczos[d]	FEM[a]	Difference[b]
1	1.9922357634	1.9922357634	1.9922357634	0.0
2		4.3051384550	4.3051384553	$-3.0 \cdot 10^{-10}$
3		4.6993231357	4.6993231360	$-3.0 \cdot 10^{-10}$
4	6.8954263767	6.8954263765	6.8954263772	$-7.0 \cdot 10^{-10}$
5		7.8378702941	7.8378702962	$-2.1 \cdot 10^{-09}$
6	7.9793012472	7.9593012390	7.9593012410	$-2.0 \cdot 10^{-09}$
7		10.0165291976	10.0165292001	$-2.5 \cdot 10^{-09}$
8		10.5861882834	10.5861882862	$-2.8 \cdot 10^{-09}$
9		11.7788803250	11.7788803349	$-9.9 \cdot 10^{-09}$
10		11.8005553313	11.8005553411	$-9.8 \cdot 10^{-09}$
11		13.4155400229	13.4155400285	$-5.6 \cdot 10^{-09}$
12		14.2097757808	14.2097757915	$-1.1 \cdot 10^{-08}$
13	14.4805192	14.4819638906	14.4819639001	$-9.5 \cdot 10^{-09}$

[a]This work.
[b]Difference is taken between the results of this work and Braun *et al.*[55]
[c]Kaluza[56] calculated only the eigenstates with positive parity and exchange quantum numbers.
[d]Braun *et al.*[55]

c. 2D Hénon-Heiles Potential. An additional benchmark for a highly coupled 2D system was the extensively studied Hénon-Heiles potential,[57] given by

$$V(x,y) = \frac{1}{2}(x^2+y^2) + \lambda x\left(y^2 - \frac{x^2}{3}\right), \tag{31}$$

with $\lambda = \sqrt{0.0125}$, consistent with the choice of previous work. The eigenvalues and eigenfunctions of this system have been treated by many authors in the study of anharmonically coupled oscillators.[58–62] The FEMVib results are calculated using cubic Hermite polynomials on a 300×300 QUAD8 grid in $[-6,6] \times [-6,6]$. Table III compares results from this work with previous calculations, finding excellent agreement. The eigenvalues are labeled with the principle quantum number n and angular momentum quantum number l, as discussed

TABLE III: Selected Eigenvalues of the 2D Hénon-Heiles System

(n, l)	DP-DVR[a]	Chebyshev-Lanczos[c]	FEM[b]	Semi-classical[d]	Direct relaxation[e]	Gaussian basis[f]
$(0, 0)$	0.998595	0.998595	0.998595	0.9986	0.9988	0.9986
$(1, \pm 1)$	1.990077	1.990077	1.990077	1.9901	1.9901	1.9901
	1.990077	1.990077	1.990077		1.9901	
$(2, 0)$	2.956243	2.956243	2.956243	2.9562	2.9562	2.9562
$(2, \pm 2)$	2.985326	2.985326	2.985326	2.9853	2.9853	2.9853
	2.985326	2.985326	2.985326		2.9853	
$(6, 0)$	6.737916	6.737968	6.737859	6.7379		6.7379
$(6, \pm 2)$	6.764867	6.764871	6.764769	6.7649		6.7649
	6.764867	6.764955	6.764861			
$(6, \pm 4)$	6.853431	6.853436	6.853406	6.8534		6.8534
	6.853431	6.853453	6.853425			
$(6, \pm 6)$	6.998932	6.998933	6.998930	6.9989		
	6.999387	6.999393	6.999380	6.9994		
$(7, \pm 1)$	7.659485	7.659551	7.658584	7.6595		
	7.659485	7.660248	7.659413			
$(7, \pm 3)$	7.697721	7.698226	7.697160	7.6977		
	7.736885	7.736915	7.736852	7.7369		

[a]Degani and Tannor, Gauss-Hermite quadrature discrete variable representation.[63]
[b]This work.
[c]Braun *et al.*[55]
[d]Noid and Marcus.[58]
[e]Kosloff and Tal-Ezer.[59]
[f]Davis and Heller.[60]

by Noid and Marcus.[58]

d. 3D Anharmonic Coupled Sextic Oscillator. For a simple non-separable 3D example, we considered the potential for three coupled anharmonic sextic oscillators

$$V(x, y, z) = V_6(x) + V_6(y) + V_6(z) + xy + xz + yz. \quad (32)$$

TABLE IV: Lowest 10 Eigenvalues of the 3D Anharmonic Coupled Sextic Oscillator

i	analytical Lanczos[a]	Chebyshev/ Lanczos[b]	FEM $30 \times 30 \times 30$ grid[a]	FEM $50 \times 50 \times 50$ grid[a]
1	2.9783	2.9783	2.9786	2.9783
2		5.2960	5.2973	5.2962
3		5.2960	5.2973	5.2962
4		5.8658	5.8672	5.8660
5		7.7537	7.7562	7.7541
6		7.7537	7.7562	7.7541
7	8.0917	8.0917	8.0950	8.0921
8		8.8711	8.8771	8.8719
9		8.8711	8.8771	8.8719
10	9.1149	9.1148	9.1200	9.1155

[a]Kaluza.[56]
[b]Braun *et al.*[55]
[a]This work.

We calculated the lowest 10 eigenstates and eigenvalues using quadratic Lagrange polynomials on a $30 \times 30 \times 30$ and $50 \times 50 \times 50$ HEX27 grid in $[-4, 4] \times [-4, 4] \times [-4, 4]$. The resulting eigenvalues are shown in Table IV, and agree well with the results of Kaluza[56] and Braun *et al.*[55]

e. H_2^+. The Hamiltonian in a.u. for the adiabatic two-center, one-electron problem is given by

$$\hat{H} = -\frac{1}{2}\nabla^2 - \frac{1}{r_\mathrm{A}} - \frac{1}{r_\mathrm{A}} + \frac{1}{R}, \tag{33}$$

where R is the separation between the two hydrogen nuclei and r_A, r_B are the distances between the electron and the hydrogen nuclei. We solved the ground state energy of this system in Cartesian coordinates when $R = 2.0\,a_0$. The results, along with literature data, are listed in Table V, showing that convergence improves with increasing number of elements used (h-refinement). Cubic Hermite shape functions with C^1 continuity produce more accurate results than quadratic Lagrange shape functions when the same number of elements are used. Agreement with the previous results is good.

TABLE V: Ground State Energy of the H_2^+ System

	Number of Elements	Element Type	Energy
FEM Cubic Hermite[a]	$30 \times 30 \times 30$	HEX8	-0.598572
FEM Quadratic Lagrange[a]	$30 \times 30 \times 30$	HEX27	-0.609897
FEM Quadratic Lagrange[a]	$40 \times 40 \times 40$	HEX20	-0.600578
FEM Quadratic Lagrange[a]	$50 \times 50 \times 50$	HEX20	-0.602373
FEM[b]	165	triangles	-0.60258
Exact[c]			-0.60263

[a]This work.
[b]Ford and Levin.[64]
[c]Wind.[65]

f. H_3^{2+}. For simplicity, the one-electron, three-center H_3^{2+} problem was confined to the D_{3h} symmetry case, with Hamiltonian

$$\hat{H} = -\frac{1}{2}\nabla^2 - \frac{1}{r_\mathrm{A}} - \frac{1}{r_\mathrm{B}} - \frac{1}{r_\mathrm{C}}. \tag{34}$$

The separation between pairs of hydrogen atoms is fixed to $1.68\,a_0$. It is of theoretical and experimental interest to study this system because the H_3^+ molecule, stable in this D_{3h} geometry, may produce metastable H_3^{2+} by photoionization.[66] The ground state eigenvalues are given in Table VI. The results show a similar trend to the H_2^+ calculations in terms of the effect of *hp*-refinement on the convergence. Our results are in good agreement with the results of Ackermann *et al.*,[54] Conroy,[67] Schwartz[68] and Johnson *et al.*[69] using various numerical approaches.

g. 3D Non-Polynomial Oscillator. Varshni[70] and Witwit[71] extended the one-dimensional non-polynomial oscillator (NPO) model to three dimensions, which takes on the form

$$V(x,y,z) = x^2 + y^2 + z^2 + \frac{\lambda(x^2+y^2+z^2)}{1+g(x^2+y^2+z^2)}. \tag{35}$$

Both investigations used similar inner product perturbation techniques and achieved highly accurate results by exploiting the interchange symmetry between the non-separable Cartesian coordinates. Scherrer *et al.*[72] reduced the 3D case to 1D by expanding the eigenfunction into a radial part multiplied by a spherical harmonics, and generated an effective central-

TABLE VI: Ground State Energy of the Equilateral H_3^{2+} System

Shape Function	Number of Elements	Element Type	Energy
Cubic Hermite	$30 \times 30 \times 30$	HEX8	-1.906108205
Quadratic Lagrange	$30 \times 30 \times 30$	HEX20	-1.920153357
Quadratic Lagrange	$40 \times 40 \times 40$	HEX20	-1.908975173
Quadratic Lagrange	$50 \times 50 \times 50$	HEX20	-1.909435347
Adaptive FEM[a]			-1.909570988
STO method[b]			-1.9073
GTO method[c]			-1.90945
GTO method[d]			-1.9097

[a]Ackermann *et al.*[54]
[b]Conroy.[67]
[c]Schwartz.[68]
[d]Johnson *et al.*[69]

force potential. We calculated the lowest 8 non-degenerate eigenvalues for the 3D NPO model with $\lambda = 100$ and $g = 1$ and the results are compared to others in Table VII. The agreement is good considering that no dimensionality reduction or symmetry separation techniques were employed in the present work. However, this example demonstrates the advantages of those techniques.

h. Proton Transfer Model System. The proton-transfer reaction, usually promoted by intermolecular stretching, is an essential chemical reaction in numerous systems. Sato and Iwata[73] proposed a 2D model to elucidate the dynamics of proton transfer between two species of equal mass M, using Morse functions to parametrize the hydrogen stretching potential. The model and its coordinate system are shown in Figure 1. The kinetic energy and potential energy operators are given by

$$\hat{T} = \frac{1}{2}\left[\left(\frac{1}{m} + \frac{1}{M}\right)\frac{\partial^2}{\partial x^2} + \left(\frac{1}{M} + \frac{1}{M}\right)\frac{\partial^2}{\partial R^2} + \frac{2}{M}\frac{\partial^2}{\partial x\,\partial R}\right] \tag{36}$$

$$V = \frac{1}{2}K(R - R_e)^2 + D\left\{1 - \exp\left[-\beta\left(\frac{R}{2} + x - r_e\right)\right]\right\}^2 + D\left\{1 - \exp\left[-\beta\left(\frac{R}{2} - x - r_e\right)\right]\right\}^2. \tag{37}$$

TABLE VII: Lowest 8 Non-Degenerate Eigenvalues of the 3D NPO Model.

n	l	IPP[a]	IPP[b]	MCF (1D)[c]	FEM[d]	FEM[e]
0	0	26.7059656	26.706	26.705966	26.726626	26.708770
0	1	42.2375602	42.238	42.237560	42.280243	42.243503
1	0	53.839093	53.820	53.839093	53.927243	53.851420
0	2	55.977803	55.976	55.977804	56.026935	55.984608
1	1			64.819422	64.929988	64.835512
0	3	67.960806	67.960	67.960806	68.006404	67.967075
2	0			72.780597	72.926917	72.801498
1	2			74.437213	74.532081	74.450802

[a]Witwit, inner product perturbation method.[71]
[b]Varshni, inner product perturbation method.[70]
[c]Scherrer *et al.*, matrix-continued-fraction algorithm, results are calculated from a reduced 1D model.[72]
[d]This work, quadratic Lagrange shape functions on $30 \times 30 \times 30$ HEX27 grids.
[e]This work, quadratic Lagrange shape functions on $50 \times 50 \times 50$ HEX27 grids.

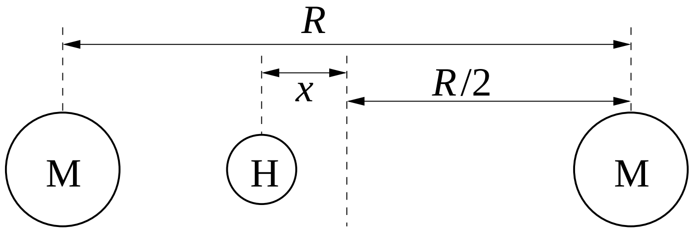

FIG. 1: Coordinate system of the proton transfer model.

Because the model coordinates x and R are not orthogonal, there is a coupling term in the kinetic energy operator. The parameters used in the model Hamiltonian are taken from Sato and Iwata.[73] The PES has two minima because the two Morse oscillators are symmetric in the coordinate x and share one transition state. The barrier height is about $1300\,\text{cm}^{-1}$.

We solved the model Schrödinger equation using both quadratic Lagrange and cubic Hermite polynomials on 100×100 QUAD8 grid over the domain $[-0.8 < x < 0.8, 2.5 < R < 3.35]$. The results are shown in Table VIII and compared to Sato and Iwata's results, calculated by the FEM approach using linear Lagrange polynomials on a 557×557 grid. The results are in excellent agreement at all energy levels. Results from this work converge

TABLE VIII: Lowest 17 Eigenvalues of the Proton Transfer Model Hamiltonian.

grid:	557×557	100×100	100×100
polynomial:	linear Lagrange[a]	cubic Hermite[b]	quadratic Lagrange[b]
v	E(v.u.)[c]	E(v.u.)[c]	E(v.u.)[c]
1	740.12	740.11	740.11
2	743.40	743.39	743.39
3	751.97	751.96	751.96
4	755.90	755.89	755.89
5	763.94	763.91	763.91
6	768.43	768.40	768.40
7	774.60	774.59	774.59
8	776.03	775.99	775.99
9	780.97	780.91	780.91
10	787.83	787.76	787.76
11	788.68	788.62	788.62
12	793.54	793.43	793.44
13	797.08	797.06	797.06
14	800.17	800.05	800.05
15	802.19	802.11	802.11
16	806.15	805.95	805.96
17	810.38	810.33	810.33

[a]Sato and Iwata.[73]
[b]This work.
[c]Energies are calculated in vibrational atomic units (1 v.u. = 33.715 cm^{-1}).

with fewer grids by using a higher polynomial order.

i. Hydrogen Difluoride Anion (FHF^-). The FHF^- anion provides a prime example of a symmetric, hydrogen-bonded system, as attested by a considerable theoretical and experimental literature. It features the strongest and shortest hydrogen bond in any chemical species, having a F–F separation of 2.2777 Å[74] and a hydrogen bond dissociation energy of 45.8 kcal/mol.[75] Three fundamental bands, ν_1 at 583 cm^{-1} (symmetric stretching), ν_2 at

$1286\,\mathrm{cm}^{-1}$ (bending), and ν_3 at $1331\,\mathrm{cm}^{-1}$ (antisymmetric stretching), and one overtone band, $\nu_1 + \nu_3$, have been assigned in the infrared spectrum.[76]

The vibrational problem for the FHF^- system has been probed theoretically by many authors using different numerical techniques on two and three dimensions. Stare and Balint-Kurti[19] performed a 2D Fourier Grid Hamiltonian (FGH) calculation on the collinear FHF^- in both orthogonal and non-orthogonal stretching internal coordinates. Spirko *et al.*[77] solved the 3D Watson isomorphic Hamiltonian[78] on a sophisticated set of rectilinear vibrational coordinates. Yamashita *et al.*[79] used a mixed discrete-variable/finite-basis representation approach combined with an adiabatic separation between the "heavy-atom" (symmetric stretching) and other vibrational modes on the hyperspherical coordinates. Their findings are in good agreement with experiment, suggesting a high degree of anharmonicity for the antisymmetric stretching mode and strong coupling between the antisymmetric stretching and bending modes. The bending mode, however, exhibits virtually no deviation from harmonicity. Most recently, this system has been treated using Fourier grid[80] and vibrational self-consistent field (VSCF) calculations[81] to obtain results that agree with experiment to high precision. Table 1 of Ref. 81 contains a comprehensive review of previous results.

The PES of Stare and Balint-Kurti[19] was calculated at the MP4(SDQ)/6-311++G(2d,2p) level of theory for 422 FHF^- collinear structures by varying H–F separations r_1 and r_2 over the range 0.8–2.4 Å. We first treat this problem using the orthogonal normal coordinates, $r_1 + r_2$ and $r_1 - r_2$, and fit the PES to a 66-parameter Chebyshev series (LnX, Y) bivariate polynomial in TableCurve 3D (Fig. 2). This Chebyshev series polynomial had the highest R^2 value among over 3000 non-linear equations tested. The average absolute fitting error per point over the entire PES domain is only $1.17\,\mathrm{cm}^{-1}$. The 2D vibrational Hamiltonian was then solved on the above PES using the G-matrix elements (G^{11}=4.10526 amu^{-1} and G^{22}=0.10526 amu^{-1}) calculated by Stare and Balint-Kurti.[19] Because the orthogonal coordinates are used, the kinetic energy coupling term with G-matrix element G^{12} vanishes. A 200×200 QUAD8 grid with quadratic Lagrange shape functions is applied on the region $[1.6, 4.8] \times [-1.6, 1.6]$ and the results are shown in Table IX.

Inspired by the model Hamiltonian developed by Sato and Iwata[73] for the linear $\mathrm{M}\cdots\mathrm{H}\cdots\mathrm{M}$ system using non-orthogonal coordinates, we adopted their coordinate system in Fig. 1 and fit the PES to a second 66-parameter Chebyshev series (X, LnY) bivariate polynomial in TableCurve 3D (Fig. 3), obtaining the same $1.17\,\mathrm{cm}^{-1}$ absolute average fit-

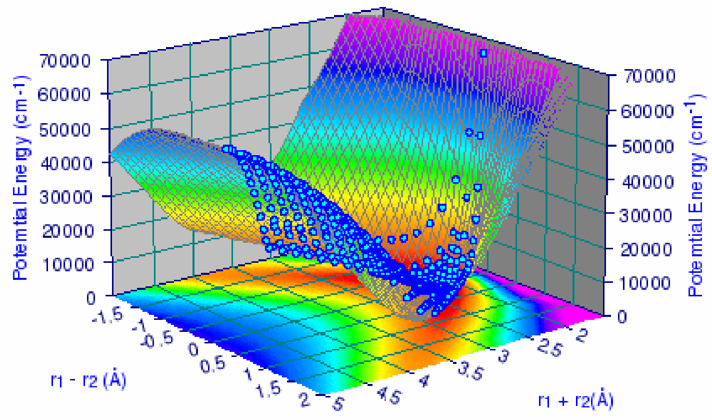

FIG. 2: FHF^- PES in orthogonal normal coordinates.

ting error per point over the domain. Because the coordinate set $\{x, R\}$ is not orthogonal, a non-zero coupling term is included in the vibrational Hamiltonian. The G-matrix elements G^{11}=0.95716 amu^{-1}, G^{22}=0.10527 amu^{-1}, and G^{12}=0.05264 amu^{-1}) are calculated from the atomic masses of H and F using Sato and Iwata's model Hamiltonian. The 2D system is solved by FEM using quadratic Lagrange shape functions on a 200×200 QUAD8 grid in the domain $[-0.8, 0.8] \times [1.6, 4.8]$. Both analyses, using either orthogonal or non-orthogonal coordinates, produce 1883201 non-zero entries for a matrix of dimension 120801, for a sparseness of 99.9871%.

Table IX shows selected computational and experimental results for comparison. The FEM calculation on the normal coordinate system yields results similar to those of previous studies, and more accurate results are obtained using Sato and Iwata's coordinate system $\{x, R\}$. The results from these 2D analyses compare favorably in accuracy to the full 3D analysis.[77] Results from this work and from Stare and Balint-Kurti[19] both predict the zero-point energy of FHF^- to be around 960 cm^{-1}.

j. Picolinic Acid N-oxide. Picolinic acid N-oxide (PANO, Fig. 4) exhibits a very short and strong intramolecular OH$\cdots$O hydrogen bond, which results in an asymmetric, single-well proton potential. PANO has been a difficult system to characterize, with inconsistent results being found among experimental and theoretical studies. For example, the most

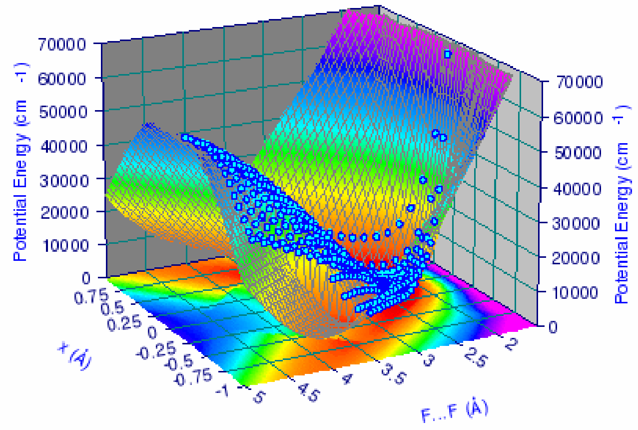

FIG. 3: FHF^- PES in x and R coordinates.

recent x-ray diffraction study of crystalline PANO indicates that the O···O distance is only 2.428 Å.[82] However, Stare and Balint-Kurti found that the O···O distance in the optimized gas-phase geometries was always greater than 2.5 Å, no matter what level of theory was used.[19] Furthermore, harmonic frequency calculations at B3LYP/6-311++G(3df,3pd), B3LYP/6-31+G(d,p) and B3LYP/6-31G(d,p) levels yield O–H stretching frequencies ν_{OH} of 2977 cm^{-1},[19] 2965 cm^{-1},[83] and 2991 cm^{-1}[84] respectively. In the experimental infrared spectrum of PANO isolated in an Ar matrix, however, Szczepaniak *et al.*[84] found no intense absorption band within 1200 cm^{-1} of the 2900 cm^{-1} region for the O–H stretch. From their experimental results and an anharmonic simulation of the normal modes, Szczepaniak *et al.* concluded that the ν_{OH} absorption intensity is redistributed into the in-plane O–H bend and the C=O stretch, which account for 59% and 45% of the band intensities at 1867 cm^{-1} and 1514 cm^{-1}, respectively. This issue has recently been revisited by Stare *et al.* in a combined experimental and CPMD analysis of PANO in the solid state.[85] Here, we present a 2D analysis using the potential surfaces for PANO calculated by Stare and Balint-Kurti[19] and by Stare and Mavri.[83]

The first PES was calculated using the Car-Parrinello Molecular Dynamics program.[19,86] Stare and Balint-Kurti performed single point energy calculations on 340 distinct structures, varying the O–H distance (0.8–1.75 Å) and the COH angle (70°–150°). We fit this PES to

TABLE IX: Selected Vibrational Energies of FHF^- (cm^{-1}).

Method	ZPE	ν_1	ν_3	$\nu_1 + \nu_3$
harmonic[a]		645	1041	1686
FGH[b]	961	592	1369	1891
rectilinear coords[c]		580	1315	1814
DVR[d]		595	1374	1904
Fourier grid[e]		593	1448	1977
VCI[f]		580	1313	1837
FEM normal coords[g]	960	593	1369	1892
FEM $\{x, R\}$[h]	929	584	1319	1841
Experimental[i]		583	1331	1848

[a]Calculated at the MP4(SDQ)/6-311++G(2d,2p) level.[19]
[b]Stare and Balint-Kurti.[19]
[c]Spirko *et al.*[77]
[d]Yamashita *et al.*[79]
[e]Elghobashi and González[80]
[f]Hirata *et al.*[81]
[g]This work.
[h]This work.
[i]Kawaguchi and Hirota.[74,76]

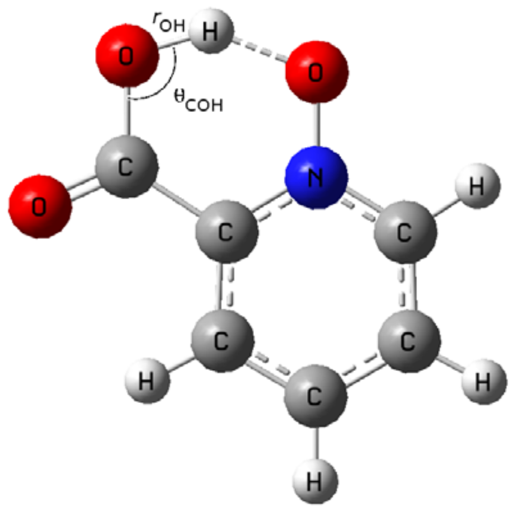

FIG. 4: Structure of picolinic acid N-oxide (PANO) and the O–H stretching and bending internal coordinates.

TABLE X: Calculated Fundamental Vibrational Frequencies (cm^{-1}) in Crystal PANO

	FGH[a]		FEM[b]	
	ν_{COH}	ν_{OH}	ν_{COH}	ν_{OH}
full Hamiltonian	1299	1767	1283	1757
equilibrium G^{rs}	1386	1831	1351	1826
averaged G^{rs}			1284	1717
variable G^{rs}, $\partial G^{rs}/dq = 0$			1264	1763

[a]Stare and Balint-Kurti.[19]
[b]This work.

a Chebyshev series X, LnY bivariate polynomial. To take into account the coordinate dependency of the G-matrix elements, we also calculated the G-matrix elements at each of the optimized geometries and fit each to a Chebyshev series polynomial, from which analytical derivatives of the G-matrix elements were available. The vibrational Hamiltonian was then solved by FEM on a 200×200 QUAD8 grid over the PES domain using quadratic Lagrange shape functions under different approximations for the G-matrix elements: (*i*) using the full Hamiltonian with dynamic G-matrix elements G^{rs}, (*ii*) fixing the three G^{rs} values to the equilibrium values, (*iii*) fixing the G^{rs} values to the values averaged point-by-point over the domain of the PES, and (*iv*) varying the G^{rs} but omitting their derivatives in Eq. 11. The results are shown in Table X.

The results using the full Hamiltonian obtained by FEM and by FGH are in good agreement. For the fixed G^{rs} calculations, the pointwise averaged G^{rs} values yield better agreement with the full Hamiltonian than the equilibrium G^{rs} values. The effect of excluding the G^{rs} derivatives from the Hamiltonian in this case is small, comparable to the effect of fixing the G^{rs} values. This occurs because this 2D model focuses on motion of the proton, so the overall system reduced mass remains nearly constant.

The second calculation is carried out on the 2D, B3LYP/6-31+G(d,p) PES of Stare and Mavri,[83] spanning a rectangular grid of 788 points varying the O–H bond length (0.8–3.15 Å) and O$\cdots$O distance (2.0–3.7 Å). We again fit the PES and G^{rs} to Chebyshev series (X, LnY) bivariate polynomials and solve the full vibrational Hamiltonian using FEM on a 200×200 QUAD8 grid with quadratic Lagrange shape functions. The results are shown in Table XI.

The fundamental frequencies for the O–H stretch are in very good agreement among different calculations. The discrepancy in the frequencies for the O$\cdots$O stretch as calculated in this work and by Stare and Mavri[83] may be caused by differences in the PES fitting schemes. The previous study fitted the PES to a shifted Gaussian type function, which introduced an absolute average fitting error per point of 55.75 cm^{-1},[83] whereas the Chebyshev series polynomial employed in this work has an average fitting error of 9.4 cm^{-1}. Inaccuracies near the PES minimum, where the lowest eigenvalues are determined, may play a significant role in these results. Furthermore, the reduced masses were previously fixed to 1 amu for the O–H stretch and to 20 amu for the O$\cdots$O stretch.[83] By using the full Hamiltonian (Eq. 10), we account for subtle effects on the G^{rs} values, including the reduced mass variation at different geometries. The average G^{22} value is found to be 0.06245 amu^{-1}, suggesting that a reduced mass less than 20 amu would be more appropriate for the O$\cdots$O stretch.

Both 2D analyses produce consistent results with the previous numerical approaches. However, PANO is apparently subject to strong mixing of the O-H stretch with other in-plane vibrations.[84] The predicted O-H stretch frequencies at 1757 cm^{-1} and 1741 cm^{-1} successfully approximate the experimental 1737 cm^{-1} band, which contains the greatest contribution from the O-H stretch. On the other hand, the crystal model predicts a fundamental frequency of 1283 cm^{-1} for the COH bend, which should correspond to the 1514 cm^{-1} band observed experimentally. There is even more uncertainty in the O$\cdots$O stretch, because no experimental data is recorded below 550 cm^{-1}. Szczepaniak *et al.* identified this coordinate as involved in two different normal modes with fundamental frequencies of 390 cm^{-1} and 274 cm^{-1},[84] which encompass the value of about 350 cm^{-1} found in our analysis.

k. The 2D Phenyl Torsions in trans-Stilbene. Chiang and Laane[87] carried out an extensive study of the the phenyl torsions in *trans*-stilbene (Fig. 5) and the torsion about the C=C bond. Based on symmetry considerations, the PES function is selected to take the form

$$V(\phi_1, \phi_2) = \frac{V_2}{2}\left[2 + \cos(2\phi_1) + \cos(2\phi_2)\right] + V_{12}\left[\cos(2\phi_1)\cos(2\phi_2)\right] + V'_{12}\left[\sin(2\phi_1)\sin(2\phi_2)\right], \tag{38}$$

where ϕ_1 and ϕ_2 are the phenyl torsional angles, V_2 determines the torsional barrier, and V_{12} and V'_{12} represent the potential energy coupling between the two rotors. The point $\phi_1 = \phi_2 = 0$ corresponds to the conformation where both phenyl rings are perpendicular to

TABLE XI: Calculated Fundamental Vibrational Frequencies (cm^{-1}) in Gas Phase PANO

	FGH[a]		FEM[b]	
	ν_{OH}	ν_{OO}	ν_{OH}	ν_{OO}
full Hamiltonian	1733	278	1741	353
equilibrium G^{rs}			1729	350
averaged G^{rs}			1732	350
variable G^{rs}, $\partial G^{rs}/dq = 0$			1730	349

[a]Stare and Balint-Kurti.[19]
[b]This work.

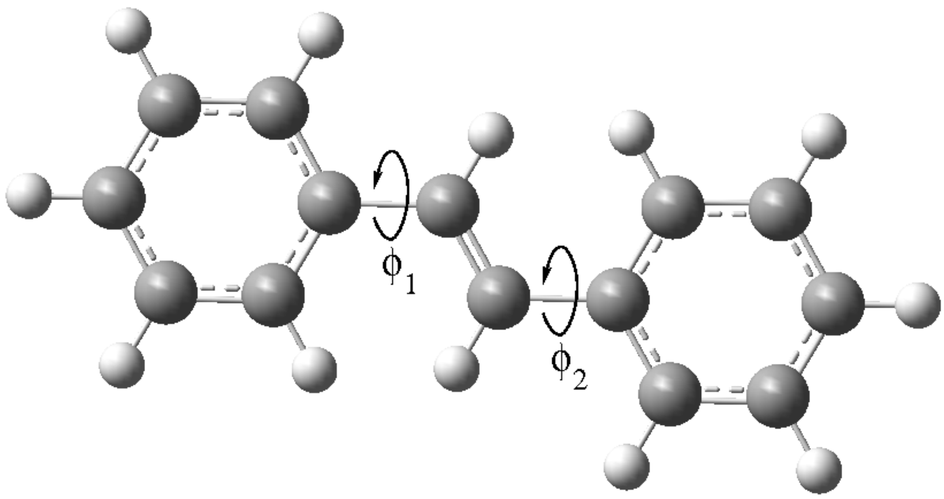

FIG. 5: The phenyl rotors in *trans*-stilbene.

the CCCC plane, and $\phi_1 = \phi_2$ corresponds to the two rings lying in parallel planes.

Chiang and Laane[87] derived the G-matrix element functions for the kinetic energy operator based on the vector method[31,88]:

$$G^{ij} = G^{ij}_{(0)} + G_{(2)}\left[\cos(2\phi_1) + \cos(2\phi_2)\right] + G_{(4)}\left[\cos(4\phi_1) + \cos(4\phi_2)\right] + G_{(c)}\cos(2\phi_1)\cos(2\phi_2) + G_{(s)}\sin(2\phi_1)\sin(2\phi_2). \quad (39)$$

Since ϕ_1 and ϕ_2 are equivalent, G^{11} and G^{22} are identical functions. Parameters for the potential and kinetic energy models were taken from Chiang and Laane for both the S_0 ground and S_1 excited states.[87]

TABLE XII: Observed and Calculated Frequencies (cm^{-1}) for the Phenyl Rotations.

state		S_0			S_1	
(v_{37}, v_{48})	Expt[a]	variable G^b	constant G^b	Expt[a]	variable G^b	constant G^b
(2,0)	9	8.9	9.1	35	35.1	35.1
(4,0)	19	20.0	20.2	70	70.0	70.1
(6,0)	31	32.3	32.7		104.8	104.4
(8,0)	45	45.7	46.2	142	139.5	139.0
(10,0)	59	60.0	60.5			
(12,0)	76	75.0	75.6			
(0,2)	118	117.8	111.6	110	110.5	104.9
(4,2)	133	134.2	128.8	146	144.9	139.7
(8,2)	160	158.6	159.5	179	179.2	174.2

[a]Chiang and Laane.[87]

[b]This work. Constant G calculations used only the leading coefficients $G^{11}_{(0)}$ and $G^{12}_{(0)}$.

The VSE was solved on a 200 × 200 QUAD8 grid over the region $[0, \pi] \times [-\pi, 0]$ using quadratic Lagrange polynomials. The results appear in Table XII. The v_{37} and v_{48} modes correspond to the orthogonal antisymmetric and symmetric torsions. The agreement between calculated and observed energy levels is excellent. In the FEM constant-G calculation, the G-matrix elements were set equal to $G^{ij}_{(0)}$, which dominate Eq. 39. The results show that variation of the system mass does not have a large impact on the calculated energy levels.

IV. CONCLUSION

We have developed a program suite for determining the vibrational eigenvalues and eigenstates on an arbitrary, multi-dimensional, anharmonic, and coupled molecular PES. The vibrational Hamiltonian is formulated and solved within the FEM framework, which combines advantages of grid-based and basis set-based approaches, and enables high accuracy through global *hp*-refinement. The large generalized eigenvalue problem is solved using the Jacobi-Davidson algorithm. The approach has been successfully tested on several systems with diverse and highly anharmonic surfaces, parametrized using bond lengths, bond angles, torsions, and linear combinations of these.

Further development is needed in a few areas. (*i*) The methods described in this work can be applied to any bounded VSE, including strongly hindered torsions as in stilbene, but we have not yet formulated the scripts to handle periodic coordinates. This would allow the accurate modeling of torsional states at energies above the barrier to full internal rotation. (*i*) Once the PES is available, fitting of the points to an analytical function is not yet straightforward in multiple dimensions. A desirable alternative is a reliable multi-dimensional interpolation using spline or weighted techniques[5] which can be constructed within the framework of the integration scheme. (*ii*) Singularities in the G-matrix elements can be avoided by careful choice of an appropriate coordinate system, and it may be beneficial to explore non-traditional coordinate systems such as the Radau vectors,[89] scattering coordinates,[90,91] valence coordinates,[92] Pekeris-Jacobi coordinates[93] or even mixed coordinate systems. Significant advantages can be gained, including the possibility of evaluating the exact kinetic energy operator and taking into account the symmetry or the constraints of the process under study more efficiently. (*iii*) The current FEM framework is designed to model dynamics up to three dimensions, and new finite element types need to be developed to solve the VSE over more coordinates. Recent higher dimension calculations employ the vibrational self-consistent field (VSCF) method,[94,95] the correlation-corrected VSCF (CC-VSCF)[96,97] and the Jacobi-Wilson method.[98,99] Many of these methods are based on a variant of multi-dimensional DVR with a contracted basis set approach[100–103] for the integration in hyperspace and a block Lanczos or Davidson algorithm for matrix diagonalization. Other schemes may include the quadrature discretization method (QDM)[104] and the discrete singular convolution (DSC).[105]

While a user-friendly package is in development by the authors, the current set of implementation instructions and accompanying scripts for this protocol is available on request.

Acknowledgments

The authors thank Charles Orr for contributions towards the integrated packaging of this approach. Financial support of the Slovenian Research Agency (program code P1-0012) is gratefully acknowledged. ALC thanks the National Science Foundation for partial support (grant CHE-0719575), the SDSU CSRC for computational resources, and Dr. James Otto for instrument support.

APPENDIX A: LIBMESH IMPLEMENTATION

The LibMesh library[42] is an open source software tool for numerical simulation of partial differential equations on serial and parallel platforms, using the finite element method and developed in C++. It provides a C++ interface to the user, simplifying many programming details. LibMesh allows discretization of one, two and three dimensional stationary and transient problems using a wide variety of finite element types and interpolation polynomials. LibMesh includes interfaces for standard high performance libraries such as SLEPc[106], incorporating linear equation and eigenvalue solvers. The choice of appropriate solvers is made by the user at runtime. The PETSc and LASPack packages are integrated into LibMesh, providing several linear equation solvers, including GMRES, CG, Bi-CGSTAB, and QMR.

The rich selection of finite element types in LibMesh simplifies the definition of the global basis functions and the approximation over arbitrary domains. Because the domain in the context of the molecular vibrational problem is in conventional shape, (*e.g.*, line for 1D, square or quadrilateral for 2D and hexahedral in 3D), these elements are our first choice. The domain discretization is handled by the *Mesh* and *Elem* classes in LibMesh. The discretization is composed of elements and nodes which are stored in the mesh, but the manner in which these data are stored is encapsulated by abstract classes with implementation-independent interfaces. This data encapsulation has allowed for refactoring of the mesh class with minimal impact on the external application programming interface.

Following the partitioning of the domain into the elements, the degrees of freedom (DOFs, equal to the number of global basis functions) are numbered consecutively. The most common implementation uses standard Lagrange elements with nodal value degrees of freedom. Each DOF is also associated with one particular entry in the eigenvectors. The index of that entry corresponds to the index i of the global basis function ϕ_i. Because the DOFs correspond to values of the function at particular nodes, the DOFs are called node variables.

The *DofObject* class handles these different types of degrees of freedom generically. Examples of *DofObjects* are element interiors, faces, edges, and vertices. An element interior has associated degrees of freedom for those shape functions whose support is contained within the element. Face degrees of freedom correspond to shape functions contained within the two elements sharing a face, edge degrees of freedom correspond to shape functions for all elements sharing an edge, and vertex degrees of freedom correspond to shape functions supported on all elements sharing a single vertex.

The LibMesh library provides a number of interpolation polynomial functions to approximate the solution. The classic first-and second-order Lagrange polynomials are supported, as well as C^0 hierarchic polynomials of arbitrary order. Mapping between physical and computational space is performed with the Lagrange basis functions that are natural for a given element. For example, mapping of a three-node triangle is performed with the linear Lagrange basis functions, while a 27-node hexahedral element is mapped with a tri-quadratic Lagrange basis. For many mesh geometries, quadratic Lagrange elements are only mapped linearly from computational space. Provisions are made in the library to detect this and use the minimal polynomial degree required for an accurate map.

Support for C^1 continuous elements is provided in the library. Clough-Tocher and reduced Clough-Tocher[107] triangular macroelements can be generated on arbitrary 2D meshes, as well as tensor products of cubic or higher Hermite polynomials on rectilinear meshes in up to 3 dimensions. Either choice of element gives a function space with continuous values and first derivatives, suitable for the solution of fourth-order problems.

Discontinuous finite element spaces are also supported. For these approximation spaces the degrees of freedom are wholly owned by the elements. The library offers monomial function bases for these spaces. LibMesh also provides higher order interpolation functions such as Bernstein and SZABAB polynomials.

The user specifies the shape function family and the initial approximation order to be used for each variable in a system. The abstract *FEBase* class provides the generic interface for all polynomial families, and specific cases are instantiated with template specialization. The *FEBase* class provides essential data for matrix assembly routines, such as shape function values and gradients, the element Jacobian, and the location of the quadrature points in physical space. These calculations were implemented in the library to simplify users' physics code, but as an additional benefit this modularity has allowed many LibMesh upgrades, from C^1 function spaces to p (polynomial order) adaptivity support, to be accessible to users without requiring changes to their physics code. C++ templates are used extensively in the finite element hierarchy to reduce the potential performance overhead of virtual function calls.

APPENDIX B: SOLUTION TO THE GENERALIZED EIGENVALUE PROBLEM

The Jacobi-Davidson algorithm[50] borrows ideas from Jacobi's Orthogonal Component Correction (JOCC) and the Davidson algorithms[108] to calculate eigenvalues and eigenvectors of symmetric diagonal dominant matrices. Davidson's method is often used in quantum chemistry applications where the matrices are large, symmetric and strongly diagonally dominant. It is reported that for these applications the Davidson method is substantially faster than the Lanczos method[108], and it can be extended to matrices that are not diagonally dominant. The Jacobi-Davidson algorithm adopts Jacobi's idea to keep the correction orthogonal to the eigenvector approximation. The Jacobi-Davidson algorithm incorporates the orthogonality requirement into the correction equation (as in JOCC) instead of explicit post-orthogonalization (as in the Davidson method). Geus[109] and others[110] describe an efficient implementation of the Jacobi-Davidson algorithm for the symmetric eigenvalue problem (JDSYM).

The generalized eigenvalue problem may be written

$$\boldsymbol{A}x = \lambda \boldsymbol{M}x, \tag{B1}$$

with a real, symmetric matrix $\boldsymbol{A}$ and a real, symmetric and positive definite matrix $\boldsymbol{M}$. Equation B1 has the same eigensolutions as the standard eigenvalue problem

$$\boldsymbol{M}^{-1}\boldsymbol{A}x = \lambda x. \tag{B2}$$

Then two matrices $\boldsymbol{X}$ and Λ exist such that

$$\boldsymbol{X}^T\boldsymbol{A}\boldsymbol{X} = \Lambda \text{ and } \boldsymbol{X}^T\boldsymbol{M}\boldsymbol{X} = \boldsymbol{I}. \tag{B3}$$

Λ is a diagonal matrix holding the eigenvalues λ_k of $\boldsymbol{M}^{-1}\boldsymbol{A}$ on its diagonal. The columns of x_k of $\boldsymbol{X}$ are the associated eigenvectors of $\boldsymbol{M}^{-1}\boldsymbol{A}$.

The task of the algorithm is to compute a partial eigenvalue decomposition of dimension $k_{\max}$ for the eigenvalue problem Eq. B1. So, we look for a $\boldsymbol{Q} \in \Re^{n\times k_{\max}}$ and a diagonal matrix $\Lambda \in \Re^{k_{\max}\times k_{\max}}$, such that

$$\boldsymbol{A}\boldsymbol{Q} = \boldsymbol{M}\boldsymbol{Q}\Lambda \text{ with } \boldsymbol{Q}^T\boldsymbol{M}\boldsymbol{Q} = \boldsymbol{I}. \tag{B4}$$

The algorithm shall compute the $k_{\max}$ eigenvalues (together with associated eigenvectors), that are closest to a given target value τ. The converged eigensolutions (q_k, λ_k) are required to satisfy

$$\|r_k\|_2 = \|\boldsymbol{A} q_k - \lambda_k \boldsymbol{M} q_k\|_2 < \varepsilon; \tag{B5}$$

i.e., the 2-norm of the associated residual r_k is smaller than a given bound ε.

To improve the convergence speed of the iterative solver, we choose a preconditioner $\boldsymbol{K}$, a symmetric matrix approximating $\boldsymbol{A} - \tau\boldsymbol{M}$. The preconditioner improves the spectral properties of the matrix, reducing the number of steps required for convergence. We use black box preconditioners, operating on the system matrix only, without requiring information about the underlying problem. The Jacobi and the Symmetric Successive Over Relaxation (SSOR) iterations both fall into this category, and also belong to the family of stationary methods, *i.e.*, methods with a constant iteration matrix. Applying such a preconditioner is equivalent to performing a few steps of the iterative method. Numerical experiments have shown that the preconditioners significantly speed up the inner iteration. The SSOR preconditioner often yields significantly better performance than the Jacobi preconditioner, and has relatively modest memory requirements.

Because we deal mostly with large, symmetric, sparse matrices, we employ the Symmetric Sparse Skyline (SSS) format[111], which stores all non-zero entries of the lower triangle of the matrix. The SSS format is closely related to the Compressed Sparse Row (CSR) format, but is used for sparse *symmetric* matrices. The diagonal is stored in a separate (full) vector and only the lower triangle of the matrix is stored in CSR format. The SSS format is much more efficient than other formats because it requires about half of the memory, and the matrix-vector multiplication can be implemented to perform quickly. It is not feasible to store the global matrices $\boldsymbol{A}$ and $\boldsymbol{M}$ in SSS format during the assembly process because it is very expensive to add non-zero entries. The assembled global matrices are stored in MATLAB sparse matrix format and later converted to SSS format by the way of Matrix Market Coordinate (MMC) format because disk storage demands are usually less critical than memory.

---

* Electronic address: acooksy@sciences.sdsu.edu

[1] A. L. Cooksy, F.-M. Tao, W. Klemperer, and P. Thaddeus, J. Phys. Chem. **99**, 11095 (1995).

[2] C. L. Parker and A. L. Cooksy, J. Phys. Chem. A **103**, 2160 (1999).

[3] A. L. Cooksy, J. Phys. Chem. **102**, 5092 (1998).

[4] A. L. Cooksy, J. Am. Chem. Soc. **123**, 4003 (2001).

[5] M. G. Moreno-Armenta and A. L. Cooksy, J. Phys. Chem. A **109**, 3391 (2005).

[6] H. Voss, J. Comput. Phys. **217**, 824 (2006).

[7] S. Tonzani and C. H. Greene, J. Comp. Phys. **122**, 014111/1 (2005).

[8] W. Zheng and L.-A. Ying, Int. J. Quant. Chem. **97**, 659 (2004).

[9] I. Kanesaka and K. Kawai, J. Comp. Phys. **69**, 4323 (1978).

[10] A. Sabu, S. Kondo, N. Miura, and K. Hashimoto, Chem. Phys. Lett. **391**, 101 (2004).

[11] A. Sabu, S. Kondo, R. Saito, Y. Kasai, and K. Hashimoto, J. Chem. Phys. A **109**, 1836 (2005).

[12] T. Hrenar, H.-J. Werner, and G. Rauhut, J. Chem. Phys. **126**, 134108/1 (2007).

[13] C. Eckart, Physical Review **47**, 552 (1935).

[14] E. B. Wilson, J. C. Decius, and C. Paul, *Molecular Vibrations* (McGraw-Hill, New York, 1955).

[15] E. B. Wilson, P. C. Cross, and J. C. Decius, *Molecular Vibrations: The theory of infrared and Raman vibrational spectra* (Dover Publications, New York, 1980).

[16] B. Podolsky, Physical Review **32**, 812 (1928).

[17] V. Alexandrov, D. M. A. Smith, H. Rostkowska, M. J. Nowak, L. Adamowicz, and W. Mccarthy, J. Chem. Phys. **108**, 9685 (1998).

[18] D. Xu, Ph.D. thesis, San Diego State University, San Diego, CA (2008).

[19] J. Stare and G. G. Balint-Kurti, J. Phys. Chem. A **107**, 7204 (2003).

[20] J. Stare, J. Chem. Inf. Model. **47**, 840 (2007).

[21] L. Hedberg and I. M. Mills, J. Mol. Spectrosc. **160**, 117 (1993).

[22] J. E. Dennis and R. B. Schnable, *Numerical Methods for Unconstrained Optimization and Nonlinear Equations* (Prentice-Hall, Englewood Cliffs, 1983).

[23] P. R. Bevington, *Data Reduction and Error Analysis for the Physical Sciences* (McGraw-Hill, New York, 1969).

[24] *TableCurve 3D 4.0*, Systat, Inc. (2008).

[25] *NLREG*, Phillip H. Sherrod (2008).

[26] E. C. Kemble, *The Fundamental Principles of Quantum Mechanics* (McGraw-Hill, New York, 1937).

[27] A. Nauts and X. Chapuisat, Mol. Phys. **55**, 1287 (1985).

[28] X. Chapuisat, A. Belafhal, and A. Nauts, J. Mol. Spectrosc. **149**, 274 (1991).

[29] T. B. Malloy, J. Mol. Spectrosc. **44**, 504 (1972).

[30] R. Meyer, J. Mol. Spectrosc. **76**, 266 (1979).

[31] M. A. Harthcock and J. Laane, J. Mol. Spectrosc. **91**, 300 (1982).

[32] M. A. Harthcock and J. Laane, J. Mol. Spectrosc. **94**, 461 (1982).

[33] D. Lauvergnat and A. Nauts, J. Chem. Phys. **116**, 8560 (2002).

[34] D. Lauvergnat, E. Baloitcha, G. Dive, and M. Desouter-Lecomte, Chem. Phys. **326**, 500 (2006).

[35] E. Tsuchida and M. Tsukada, Solid State Commun. **94**, 5 (1995).

[36] E. Tsuchida, Y. Kanada, and M. Tsukada, Chem. Phys. Lett. **311**, 236 (1999).

[37] K. Tagami, E. Tsuchida, and M. Tsukada, Surf. Sci. **446**, L108 (2000).

[38] R. G. Littlejohn and M. Cargo, J. Chem. Phys. **116**, 7350 (2002).

[39] I. Degani and D. J. Tannor, J. Phys. Chem. A **110**, 5395 (2006).

[40] C.-P. Liu and J. J. S. Neto, Int. J. Quant. Chem. **95**, 103 (2002).

[41] B. I. Schneidera and L. A. Collins, J. Noncryst. Solids **351**, 1551 (2005).

[42] S. K. Benjamin, W. P. John, H. S. Roy, and F. C. Graham, Eng. with Comput. **22**, 237 (2006).

[43] G. Strang and G. Fix, *An Analysis of the Finite Element Method* (Prentice-Hall, Englewood Cliffs, NJ, 1973).

[44] H. R. Schwarz, *Finite Element Methods* (Academic Press, New York, 1988).

[45] D. Braess, *Finite Elements* (Cambridge University Press, New York, 1997).

[46] O. C. Zienkiewicz and R. L. Taylor, *The Finite Element Method* (McGraw-Hill, New York, 1989).

[47] B. D. Reddy, *Introductory Functional Analysis: With Applications to Boundary Value Problems and Finite Elements* (Springer-Verlag, New York, 1997).

[48] H. Kardestuncer and D. H. Norrie, *Finite Element Handbook* (McGraw-Hill, New York, 1987).

[49] B. N. Parlett, *The Symmetric Eigenvalue Problem* (Prentice-Hall, Englewood Cliffs, NJ, 1980).

[50] G. L. G. Sleijpen and H. A. V. D. Vorst, SIAM Journal on Matrix Analysis and Applications **17**, 401 (1996).

[51] K. J. Maschhoff and D. C. Sorensen, in *Proceedings of the Third International Workshop on Applied Parallel Computing, Industrial Computation and Optimization* (Springer-Verlag, London, 1996), p. 478.

[52] D. Xu and A. L. Cooksy, J. Molec. Struct. (THEOCHEM) **815**, 119 (2007).

[53] J. R. Alvarez-Collado and R. J. Buenker, J. Comput. Chem. **13**, 135 (1992).

[54] J. Ackermann, B. Erdmann, and R. Roitzsch, J. Chem. Phys. **101**, 7643 (1994).

[55] M. Braun, S. A. Sofianos, D. G. Papageorgiou, and I. E. Lagaris, J. Comput. Phys. **126**, 315 (1996).

[56] M. Kaluza, Comput. Phys. Commun. **79**, 425 (1994).

[57] M. Hénon and C. Heiles, Astron. J. **69**, 73 (1964).

[58] D. W. Noid and R. A. Marcus, J. Chem. Phys. **67**, 559 (1977).

[59] R. Kosloff and H. Tal-Ezer, Chem. Phys. Lett. **127**, 223 (1986).

[60] M. J. Davis and E. J. Heller, J. Chem. Phys. **71**, 3383 (1979).

[61] G. Hose and H. S. Taylor, J. Chem. Phys. **76**, 5356 (1982).

[62] I. P. Hamilton and J. C. Light, J. Chem. Phys. **84**, 306 (1986).

[63] I. Degani and D. J. Tannor, J. Phys. Chem. A **110**, 5395 (2006).

[64] W. K. Ford and F. S. Levin, Phys. Rev. A **29**, 43 (1984).

[65] H. Wind, J. Chem. Phys. **42**, 2371 (1965).

[66] W. Meyer, P. Botschwina, and P. Burton, J. Chem. Phys. **84**, 891 (1986).

[67] H. Conroy, J. Chem. Phys. **41**, 1327 (1964).

[68] M. E. Schwartz, Ph.D. thesis, Vanderbilt University, Nashville, TN (1966).

[69] J. W. Johnson and R. D. Poshusta, Int. J. Quantum Chem. **11**, 885 (1977).

[70] Y. P. Varshni, Phys. Rev. A **36**, 3009 (1987).

[71] M. R. M. Witwit, J. Comput. Phys. **129**, 220 (1996).

[72] H. Scherrer, H. Risken, and T. Leiber, Phys. Rev. A **38**, 3949 (1988).

[73] N. Sato and S. Iwata, J. Chem. Phys. **89**, 2932 (1988).

[74] K. Kawaguchi and E. Hirota, J. Chem. Phys. **84**, 2953 (1986).

[75] P. G. Wenthold and R. R. Squires, J. Phys. Chem. **99**, 2002 (1995).

[76] K. Kawaguchi and E. Hirota, J. Chem. Phys. **87**, 6838 (1987).

[77] V. Spirko, A. Cejchan, and G. H. F. Diercksen, Chem. Phys. **151**, 45 (1991).

[78] J. K. G. Watson, Mol. Phys. **19**, 465 (1970).

[79] K. Yamashita, K. Morokuma, and C. Leforestier, J. Chem. Phys. **99**, 8848 (1993).

[80] N. Elghobashi and L. González, J. Chem. Phys. **124**, 174308/1 (2006).

[81] S. Hirata, K. Yagi, S. A. Perera, S. Yamazaki, and K. Hirao, J. Chem. Phys. **128**, 214305/1

(2008).

[82] T. Steiner, A. M. M. Schreurs, M. Lutz, and J. Kroon, Acta Crystallographica Section C **56**, 577 (2000).

[83] J. Stare and J. Mavri, Comput. Phys. Commun. **143**, 222 (2002).

[84] K. Szczepaniak, W. B. Person, and D. Hadzi, J. Phys. Chem. A **109**, 6710 (2005).

[85] J. Stare, J. Panek, J. Eckert, J. Grdadolnik, J. Mavri, and D. Hadži, J. Phys. Chem. A **112**, 1576 (2008).

[86] R. Car and M. Parrinello, Phys. Rev. Lett. **55**, 2471 (1985).

[87] W.-Y. Chiang and J. Laane, J. Chem. Phys. **100**, 8755 (1994).

[88] J. Laane, M. A. Harthcock, P. M. Killough, L. E. Bauman, and J. M. Cooke, J. Mol. Spectrosc. **91**, 286 (1982).

[89] F. T. Smith, Phys. Rev. Lett. **45**, 1157 (1980).

[90] A. M. Arthurs and A. Dalgarno, Proc. Royal Soc. London. Series A **256**, 540 (1960).

[91] J. Tennyson, Computer Physics reports **4**, 1 (1986).

[92] M. J. Bramley and N. C. Handy, J. Chem. Phys. **98**, 1378 (1993).

[93] X. G. Wang and J. T. Carrington, Can. J. Phys. **79**, 623 (2001).

[94] J. M. Bowman, Acc. Chem. Res. **19**, 202 (1986).

[95] M. A. Ratner and R. B. Gerber, J. Phys. Chem. **90**, 20 (1986).

[96] J. O. Jung and R. B. Gerber, J. Chem. Phys. **105**, 10332 (1996).

[97] J. O. Jung and R. B. Gerber, J. Chem. Phys. **105**, 10682 (1996).

[98] C. Leforestier, A. Viel, F. Gatti, C. Munoz, and C. Iung, J. Chem. Phys. **114**, 2099 (2001).

[99] F. Ribeiro, C. Iung, and C. Leforestier, J. Chem. Phys. **123**, 054106 (2005).

[100] J. C. Light, I. P. Hamilton, and J. V. Lill, J. Chem. Phys. **82**, 1400 (1985).

[101] R. A. Friesner, J. A. Bentley, M. Menou, and C. Leforestier, J. Chem. Phys. **99**, 324 (1993).

[102] X.-G. Wang and J. T. Carrington, J. Chem. Phys. **117**, 6923 (2002).

[103] H. Wei and J. T. Carrington, J. Chem. Phys. **101**, 1343 (1994).

[104] B. D. Shizgal and H. Chen, J. Chem. Phys. **104**, 4137 (1996).

[105] G. W. Wei, J. Chem. Phys. **110**, 8930 (1999).

[106] V. Hernandez, J. E. Roman, and V. Vidal, ACM Transactions on Mathematical Software **3**, 351 (2005).

[107] P. G. Ciarlet, *The Finite Element Method for Elliptic Problems* (North-Holland, Amsterdam,

1978).

[108] E. R. Davidson, Computers in Physics **7**, 519 (1993).

[109] P. Arbenz and R. Geus, Numerical Linear Algebra with Applications **6**, 3 (1999).

[110] Z. Bai, J. Demmel, J. Dongarra, A. Ruhe, and H. van der Vorst, *Templates for the Solution of Algebraic Eigenvalue Problems: a Practical Guide* (SIAM, Philadelphia, 2000).

[111] Y. Saad, Tech. Rep., Research Institute for Advanced Computer Science, NASA Ames Research Center, Moffet Field, CA (1990).